

Observation of chiral magneto-transport in RPtBi topological Heusler compounds

Chandra Shekhar,¹ Ajaya K. Nayak,^{1,2} Sanjay Singh,¹ Nitesh Kumar,¹ Shu-Chun Wu,¹ Yang Zhang,^{1,3} Alexander C. Komarek,¹ Erik Kampert,⁴ Yurii Skourski,⁴ Jochen Wosnitza,⁴ Walter Schnelle,¹ Alix McCollam,⁵ Uli Zeitler,⁵ Jürgen Kübler,⁶ S. S. P. Parkin,² Binghai Yan,^{1,7,8} C. Felser^{1*}

¹Max Planck Institute for Chemical Physics of Solids, 01187 Dresden, Germany

²Max Planck Institute of Microstructure Physics, 06120 Halle, Germany

³Leibniz-Institut für Festkörper- und Werkstoffforschung 01069 Dresden, Germany

⁴Dresden High Magnetic Field Laboratory (HLD-EMFL), Helmholtz-Zentrum Dresden-Rossendorf, 01328 Dresden, Germany

⁵High Field Magnet Laboratory (HFML - EMFL), Radboud University, Toernooiveld 7, 6525 ED, Nijmegen, The Netherlands.

⁶Institut für Festkörperphysik, Technische Universität Darmstadt, 64289 Darmstadt, Germany

⁷Institute of Condensed Matter Physics and Photon Science, ShanghaiTech University, Shanghai 200031, China

⁸Max Planck Institute for the Physics of Complex Systems, 01187 Dresden, Germany

Topological materials ranging from topological insulators(1, 2) to Weyl(3-7) and Dirac semimetals(8, 9) form one of the most exciting current fields in condensed matter research. Many half-Heusler compounds have been theoretically predicted to be topological semimetals. Of these many are also superconductors, are magnetic or show Kondo behavior(10-12). Recently, experimental evidence was found for an unusual topological surface state(13), and a chiral anomaly(14) that is a characteristic feature of a Weyl semimetal in lanthanide half-Heusler compounds. Here we demonstrate that the antiferromagnetic Heusler compounds GdPtBi and NdPtBi show three signatures of a chiral anomaly, namely, a large non-saturated negative magnetoresistance for fields up to 60 T, a quadratic field dependence of the magneto-conductivity, and an unusual intrinsic anomalous Hall effect, all three observed far above the magnetic ordering temperature. We show that the Weyl points are induced in a magnetic field via exchange-splitting of the conduction bands. A generic, complex magneto-transport phase diagram for magnetic topological Heusler compounds is presented that is distinguished from that of non-magnetic Heusler compounds, such as YPtBi. Our observations open the path for the study of the quantum anomalous Hall effect in

magnetic Heusler compounds(15) and of Majorana fermions in topological Heusler compounds with co-existing superconductivity(16).

Heusler compounds are a unique class of materials which allow for a controllable tuning of their structural (e.g. cubic to tetragonal) and physical functionalities, to allow for topological insulators(10-12), compensated ferrimagnets(17), half-metallic ferromagnets(18), non-collinear spin structures(19), unconventional superconductivity in non-centrosymmetric crystals (20), and an exotic anomalous Hall effect(21, 22). Within the extended class of half-Heusler semiconductors and semimetals, around fifty compounds have been predicted to be topological insulators with an inverted band structure(10-12). The associated topological surface states have recently been observed by angle-resolved photoemission studies(13). In this work, we utilize such multi-functionality to design a half-Heusler family of topological Weyl semimetals (WSMs) by combining magnetism with band inversion.

The WSM is a three-dimensional (3D) analogue of graphene, in which the conduction and valence bands disperse linearly through nodes, called Weyl points, in momentum space(4). Weyl points are singular monopoles of the Berry curvature, an intrinsic property of the wave function, with “+” or “-” chirality, and thus always come in pairs. A hallmark of a WSM is the existence of Fermi-arc type surface states(4), which connect the Weyl nodes in each pair. The chiral anomaly results from topological charge pumping between Weyl points within a pair, which is characterized by negative longitudinal magneto-resistance (MR). The recent discovery of time-reversal-invariant WSMs in the TaAs-type transition-metal monpnictides(3, 5) was demonstrated via the observation of Fermi arcs(23, 24) and a possible chiral MR(11, 25, 26). Moreover, time-reversal breaking WSMs are anticipated to exhibit an anomalous Hall effect due to the net Berry flux that is proportional to the separation of Weyl points with opposite chirality(13, 27), but await experimental verification.

In this paper we consider magnetic lanthanide half-Heusler compounds formed from RPtBi , where R is a lanthanide or Y. These compounds have a non-centrosymmetric lattice (space group No. 216, $F\bar{4}3m$). The structure of RPtBi is composed of three interpenetrating fcc lattices (Fig. 1A) so that along the [111] direction the structure can be described as a

metallic multilayer formed from successive atomic layers of rare-earth, platinum and bismuth (Fig. 1B). A band inversion between the Γ_8 and Γ_6 bands results in a gapless semimetal with degenerate Γ_8 bands at the Fermi energy for all lanthanide RPtBi compounds(10). When R=Y the compound is non-magnetic but substitution of Y with most of the lanthanides gives rise to magnetism. For example, when Y is substituted by Gd or Nd, GdPtBi and NdPtBi exhibit magnetism arising from their 4f electrons but the Γ_8 - Γ_6 band inversion is preserved. GdPtBi(28, 29) as well as NdPtBi(30) are antiferromagnetic (AFM) at low temperatures below their corresponding Neel temperatures, $T_N = 9.0$ K and 2.1 K, respectively. The magnetic structure of these compounds are different: GdPtBi is a type II antiferromagnet(28, 29) whereas the magnetic structure of NdPtBi is of type I(30), reflecting that the concrete magnetic ordering below the Néel temperature does not influence the Weyl physics. Additionally, one should be aware of that the size, anisotropy moments and the degeneracy are distinguished for neodymium and gadolinium.

Recently a negative MR was reported in GdPtBi(14) when a magnetic field B was applied parallel along the current direction. This was attributed to a chiral anomaly associated with a WSM. However, the existence of Weyl points was attributed to an external field induced Zeeman splitting. We believe that any such effect is negligible compared to that derived from the much larger exchange-field from the 4f electrons. In the absence of an external field, the exchange fields from the sub-lattice magnetizations cancel and we find no Weyl nodes. However, in the presence of an external magnetic field, the magnetization of the Gd moments can be aligned in modest fields, as we show later, forcing GdPtBi into a “ferromagnetic” (FM) state.

We have used *ab-initio* density-functional theory to calculate the electronic structure of GdPtBi and YPtBi, as exemplary magnetic and non-magnetic compounds, respectively (see Supplementary Information for details). A schematic diagram of their relevant energy bands is shown in Fig. 1C. In GdPtBi, the Gd-*f* bands are well localized at energies below the Fermi energy, but we find a large exchange derived spin-splitting of the Γ_8 and Γ_6 bands in GdPtBi, when there is a net magnetization induced by an external magnetic field, which is absent in

YPtBi. This leads to a pair of Weyl points where the valence and conduction bands touch each other. In the fully magnetized FM state, the orientation of the magnetic moments sensitively affects the Fermi surface and changes the positions and numbers of the Weyl points. For instance, four pairs of Weyl points (see Fig. 1D) exist slightly below the Fermi energy when the magnetic moments are along the [111] direction (Fig. 1B) while six pairs of Weyl points appear at different positions in the Brillouin zone when the moments are oriented along the [001] direction.

The anomalous Hall effect (AHE) is a well-established property of ferromagnetic materials with non-zero magnetization(31). Recently, it has been shown that non-collinear antiferromagnets with zero net magnetization can produce a large AHE when their electronic structure exhibits a non-vanishing Berry-curvature (that acts like a large fictitious magnetic field)(21, 22, 32). Recent theoretical studies have predicted that a large AHE can also be realized in Weyl semimetals that exhibit a chiral magnetic anomaly, where the anomalous Hall conductance (AHC) is proportional to the separation between the Weyl nodes(27). As discussed in Fig. 1, GdPtBi is an ideal Weyl semimetal with field induced Weyl nodes near the Fermi level. To experimentally observe the anomalous Hall effect in GdPtBi we have performed Hall effect measurements as shown in Fig. 2. The Hall resistivity, ρ_{yx} , measured at different temperatures for two different GdPtBi samples with current along $[1\bar{1}0]$ and $[100]$ are shown in Fig. 2, A and D, respectively. At low temperatures ($T < 20$ K) ρ_{yx} reveals a small hump around 2 T, that shifts to higher fields as the temperature is increased. The low field, non-linear behavior of ρ_{yx} is reflected in pronounced dips at the same magnetic fields in ρ_{xx} , as can clearly be seen in Fig. 2, B and E. These anomalies in ρ_{yx} and ρ_{xx} almost disappear for $T \geq 100$ K. Consistent with the ρ_{yx} and ρ_{xx} data, the Hall conductivity, σ_{xy} , calculated for both crystals (Fig. 2, C and F) also exhibits a peak in the same H - T regime. When the moments are along [111], for example, our *ab-initio* calculations predict the separation of the Weyl points along the [111] axis is as large as 30% of the Brillouin zone width, guaranteeing an observable large AHE and chiral-anomaly-induced negative MR.

We have also performed similar transport measurements in YPtBi, as shown in Fig. 2, G to I. A one-to-one comparison of the resistivity/conductivity of YPtBi with that of GdPtBi clearly shows that no anomaly exists in the ρ_{yx} , ρ_{xx} and σ_{xy} data for YPtBi. This signifies the existence of an AHE in GdPtBi. It can be noted here that GdPtBi, which shows a Néel temperature (T_N) of approximately 9 K, does not exhibit any kind of spin-flop transition in the magnetic isotherm ($M(H)$) measurements. Therefore, it is highly unlikely that the AHE originates from any kind of magnetic transition in GdPtBi.

We measured the field dependence of ρ_{xx} at various angles, θ , between the applied field and the current direction at 2 K for three differently oriented crystals (see Figs. 3 A, C and E). When $\theta = 0^\circ$ ($I \perp B$), ρ_{xx} increases with field with a minimum at $B = 2$ T. When the field is gradually tilted towards the current direction, ρ_{xx} decreases and reaches a minimum value at $\theta = 90^\circ$ ($I \parallel B$). Irrespective of the crystallographic direction along which the current is applied, we find a similar angular dependence of ρ_{xx} with a large negative magnetoresistance for $\theta \geq 60^\circ$. Considering Fig. 3B as an example, for the case of $I \parallel B \parallel [1\bar{1}0]$, ρ_{xx} at 0 T and 9 T are 2.1 m Ω cm and 0.72 m Ω cm, respectively, that gives a MR of -65%. Interestingly, this low temperature negative MR is unsaturated up to 60 T. To explore the range of temperatures over which the negative MR is found, we measured the field dependence of ρ_{xx} at different temperatures for $\theta = 90^\circ$. As shown in Figs. 3B, 3D ρ_{xx} vs B is nearly independent of temperature up to 12 K, moderately increases with increasing temperature, and then becomes a positive magnetoresistance at ~80 K.

We have also measured the magnetotransport properties of both NdPtBi. NdPtBi shows similar angular and temperature dependent magnetotransport properties as GdPtBi. At $T = 2$ K NdPtBi exhibits a negative magnetoresistance for $I \parallel B$ of -20% in $B = 9$ T. The MR decreases with increasing temperatures. In contrast to GdPtBi and NdPtBi, YPtBi shows a positive magnetoresistance for similar temperature and field ranges. Therefore, we conclude

that the chiral anomaly is very robust and originates from the magnetic ground state of the lanthanide half-Heusler compounds.

For a better understanding of the origin of the AHE in GdPtBi, we have plotted the anomalous Hall angle (AHA) as a function of magnetic field in Fig. 4, A and C. The AHA is calculated after subtracting the normal Hall angle from the total Hall angle. Interestingly, the sample with B along $[111]$ and I along $[1\bar{1}0]$ exhibits a large peak in the AHA of ~ 0.23 for fields near $B = 2.2$ T at $T = 2$ K (Fig. 4A). With increasing temperature, the AHA decreases and the peak position shifts to higher magnetic fields. The crystal with I parallel to $[100]$ and B parallel to $[001]$ displays a peak with a lower value of AHA of ~ 0.17 near 2.2 T at 2 K (Fig. 4C). In this case the AHA decreases with temperatures and completely vanishes near 100 K.

To probe the relationship between the chiral anomaly and the AHE, we have measured the MR up to fields of 33 T with I parallel to B in both samples as shown in Fig. 4, B and D. It is very interesting to note that the sample with I parallel to $[1\bar{1}0]$ that displays the highest negative MR of $\sim 68\%$ at $T = 2.5$ K, also exhibits a maximum AHA of 0.23 at $T = 2$ K. Similarly, the $[100]$ sample with a smaller negative MR (39 %), shows a lower AHA (0.17). At $T = 100$ K, since this sample exhibits a positive MR up to $B = 18$ T, no AHA can be found at this temperature. Another interesting fact is that the peak position of the AHA nearly coincides with the field at which the MR exhibits a sudden drop. All these facts indicate that the AHE in the present sample is closely related to the negative MR and hence the existence of the chiral anomaly. This conclusion is also supported by the finding of a very small AHE in NdPtBi that displays only a negative MR of approximately 20%. In order to verify that the negative MR originates from the chiral magnetic anomaly we have fitted the inverse longitudinal resistivity with a parabolic function. Interestingly the inverse longitudinal resistivity closely follows a B^2 behavior (Fig. 4E), as predicted by theory.

From the high field magnetization measurements of GdPtBi, we found that at $T = 1.4$ K, the sample becomes fully magnetized in a field of ~ 25 T with a magnetic moment per Gd of almost $6.5 \mu_B$, which is close to that of a fully localized moment of $7.0 \mu_B$. For $T > T_N$, the

magnetization exhibits a linear behavior with magnetic fields. From the magneto-transport and magnetization data we can draw a generic phase diagram (Fig. 4F) that shows how the various physical properties of GdPtBi depend on temperature and applied field. The AHE is observed in a limited temperature range that extends from below to above T_N . On the other hand we observe a negative MR over a wide temperature range although at higher temperatures only when the applied field is high enough.

Our experimental studies show that GdPtBi and NdPtBi become Weyl semimetals when the exchange splitting of the Γ_8 and Γ_6 bands is sufficiently large to establish the Weyl nodes. This, we find, is established for applied fields only of the order of ~ 2 T. It is clear from our experiments that this is not possible from Zeeman splitting but rather the external field results in a significant alignment of the magnetization of the antiferromagnetic structure resulting in a large exchange field. Although the magnitude of this exchange field will increase beyond 2 T up to the saturation field (~ 25 T at $T = 1.4$ K), it is clear that once the exchange field is sufficiently large to reveal the Weyl modes, further increases in the exchange field do not much affect the Weyl properties. This also accounts for the observation of the Weyl properties to high temperatures well above the Néel temperature but the field required to establish the critical exchange needed will obviously be larger. We propose that the dip in resistivity and the corresponding peak Hall conductivity (or angle) with magnetic field reflect this critical exchange value and the corresponding band-gap opening. We speculate that all magnetic rare earth RPtBi and RAuSn ($R = \text{Ce-Sm, Gd-Tm}$) compounds will show related phase diagrams. For the systems CePtBi and YbPtBi the situation might be more complicated.

Methods:

Crystal growth: Single crystals of Y(Gd, Nd)PtBi were grown by the solution growth method from a Bi flux. Freshly polished pieces of Y or (Gd or Nd), Pt and Bi, each of purity $>99.99\%$, in the stoichiometric ratio (with significant excess Bi, i.e. Gd:Pt:Bi = 1:1:9) were placed in a

tantalum crucible and sealed in a dry quartz ampoule under 3 mbar partial pressure of argon. The ampoule was heated at a rate of 100 K/h up to 1473 K and soaked for 12 hours at this temperature. For crystal growth, the temperature was slowly reduced by 2 K/h to 873 K and the extra Bi flux was removed by decanting from the ampoule at 873 K. Typically we could obtain crystals, 1-5 mm in size, with a preferred growth orientation along [111], as confirmed by Laue diffraction. The methods we used follow closely those described in ref (33). The composition and structure was checked by energy dispersive X-ray analysis and Laue X-ray diffraction, respectively. The lattice parameters of the cubic structure are 6.65 Å for YPtBi, 6.68 Å for GdPtBi and 6.76 Å for NdPtBi which are consistent with previous reports(33-35).

Magnetoresistance and heat-capacity measurements: Resistivity measurements were performed in a physical property measurement system (PPMS-9T, Quantum Design,) using the ACT with rotator option. Heat capacity was measured by a relaxation method (HC option, PPMS, Quantum Design). 33 T static magnetic field measurements were performed at the High Field Magnet Laboratory HFML-RU/FOM in Nijmegen, and the 60 T pulsed magnetic field experiments were carried out at the Dresden High Magnetic Field Laboratory HLD at HZDR; both laboratories are members of the European Magnetic Field Laboratory (EMFL). Samples with bar shape of different crystalline orientations were cut from large single crystals using a wire saw. The orientation of these crystals was verified by Laue X-ray diffraction measurements and their physical dimensions are (width×thickness×length) 0.57×0.15×2.0 mm³ for GdPtBi, 0.63×0.24×1.21 mm³ for NdPtBi and 0.85×0.21×1.6 mm³ for YPtBi. The linear contacts were made on the orientated crystals by silver paint and 25 µm platinum wires. The resistivity (ρ_{xx}) and Hall resistivity (ρ_{yx}) were measured in 4-wires and 5-wires geometry, respectively using a current of 1.0 mA at temperature range from 2 to 300 K and magnetic fields up to 9 T. Special attention was paid to the mounting of the samples on the rotator puck to ensure a good parallel alignment of the current and magnetic field direction. The Hall resistivity contributions to the longitudinal resistivity and vice versa, due to contact misalignment, were accounted by calculating the mean resistivity of positive and negative

magnetic fields. Almost symmetrical longitudinal resistivities were obtained for positive and negative magnetic fields when current and magnetic field were parallel showing the excellent crystal and contact alignment of our samples. Otherwise the negative MR was overwhelmed by the transverse, i.e. Hall resistivity and trivial positive MR.

Density-functional calculations: Density-functional theory (DFT) calculations were performed using the Vienna *ab-initio* Simulation Package (VASP)(36) with the generalized gradient approximation (GGA)(37) of the exchange-correlation energy. The experimentally measured lattice parameter was adopted and spin-orbit coupling was included in all calculations. $10 \times 10 \times 10$ k -meshes were used for the Brillouin zone sampling. An on-site Coulomb interaction was considered for the f electrons of Gd with $U = 10$ eV. The band structures were projected to maximally localized Wannier functions(38). The chirality of the Weyl points was confirmed by identifying the source or sink type distribution of the Berry curvature.

Acknowledgements:

We acknowledge financial supports from the Max Planck Society and ERC Advanced Grant (291472 Idea Heusler). We also acknowledge support from the Dresden High Magnetic Field Laboratory (HLD) at HZDR and the High Field Magnet Laboratory (HFML-RU/FOM), members of the European Magnetic Field Laboratory (EMFL).

Author Contributions:

Competing financial interests:

The authors declare no competing financial interests.

Figure captions

Figure 1. **Crystal and band structures of Heusler Weyl semimetals.** (A) Cubic unit cell of RPtBi (R=Y, Gd or Nd). (B) View of the structure showing R-Pt-Bi type layers stacked along the [111] axis. The magnetic moments of the R atoms are shown as arrows corresponding to the fully saturated “ferromagnetic” state. (C), Schematic comparison of the calculated band structures of YPtBi and GdPtBi. The exchange field from the R moments lifts the spin-degeneracy of the Γ_8 and Γ_6 bands and induces Weyl points which are slightly below the Fermi energy: the green and red hour-glasses represent Weyl cones with opposite chiralities. (D) The distribution of Weyl points in the first Brillouin zone when the R magnetic moments are fully saturated along [111] (as shown in (B)). Green and red spheres represent “-” and “+” chirality, where the arrows are the Berry curvature vectors.

Figure 2. **Magneto-transport data for GdPtBi and YPtBi.** Field dependence of Hall resistivity (ρ_{yx}) measured for $I \perp B$ for (A) GdPtBi with current along $[1\bar{1}0]$, (D) GdPtBi with current along [100], and (G) YPtBi. (B, E, H) Field dependence of transverse resistivity (ρ_{xx}) associated with the measurements in A, D and G. (C, F, I) corresponding calculated Hall conductivities (σ_{xy}) from the relation $\sigma_{xy} = \frac{\rho_{yx}}{\rho_{yx}^2 + \rho_{xx}^2}$.

Figure 3. **Angular dependence of magnetoresistance of GdPtBi and YPtBi.** Field dependent resistivity, ρ_{xx} , for GdPtBi for various θ from $\theta = 0^\circ$ ($I \perp B$) to $\theta = 90^\circ$ ($I \parallel B$) at $T = 2\text{K}$ for current along (A) $[1\bar{1}0]$, (C) [111], (E) [001], and for various temperatures at $\theta = 90^\circ$ for the same crystal orientations in (B, D and F). Corresponding data for YPtBi are shown in (G and H). The insets in the figures illustrate the field rotation with respect to current and crystallographic directions.

Figure 4. **Magnetotransport phase diagram.** Field dependence of anomalous Hall angle (AHA) calculated at different temperatures for GdPtBi with current parallel to (A) $[1\bar{1}0]$ direction and (C) $[100]$ direction. (B, D) Longitudinal MR measured at different temperatures and fields up to 33 T for the same crystal directions as shown in (A) and (C). (E) Inverse of longitudinal resistivity along with parabolic fitting at different temperatures. (F) Generic H - T phase diagram for GdPtBi showing different magnetic phases.

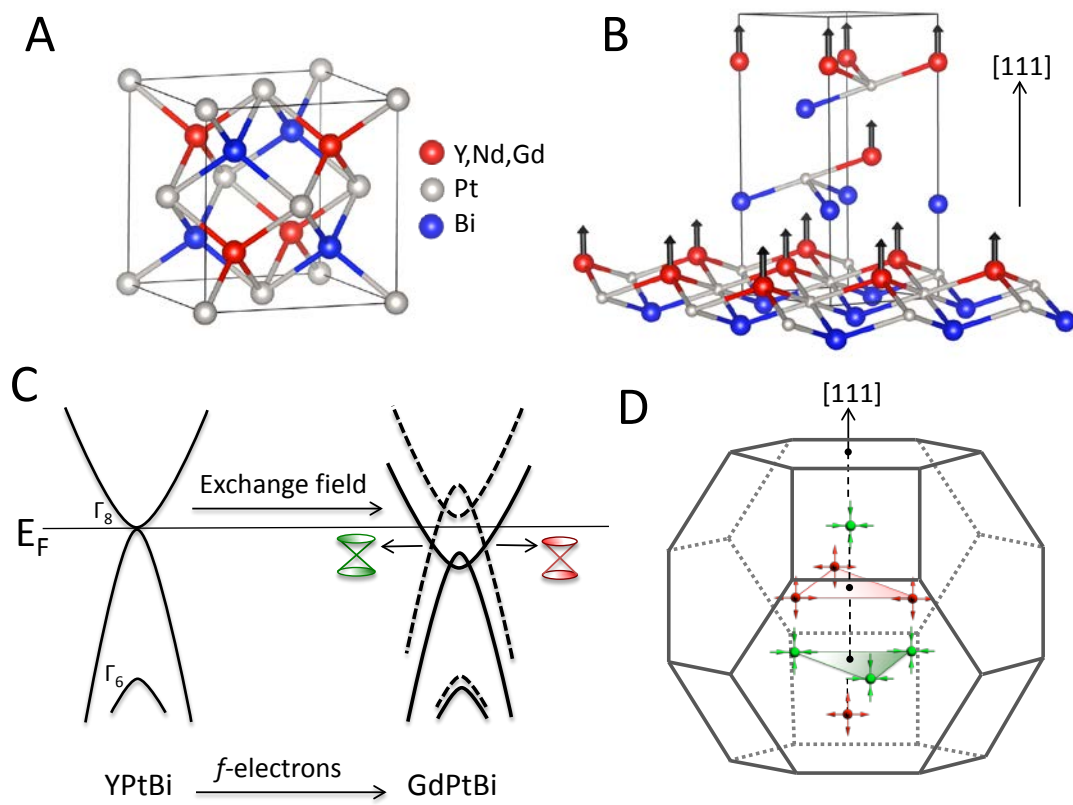


Fig. 1

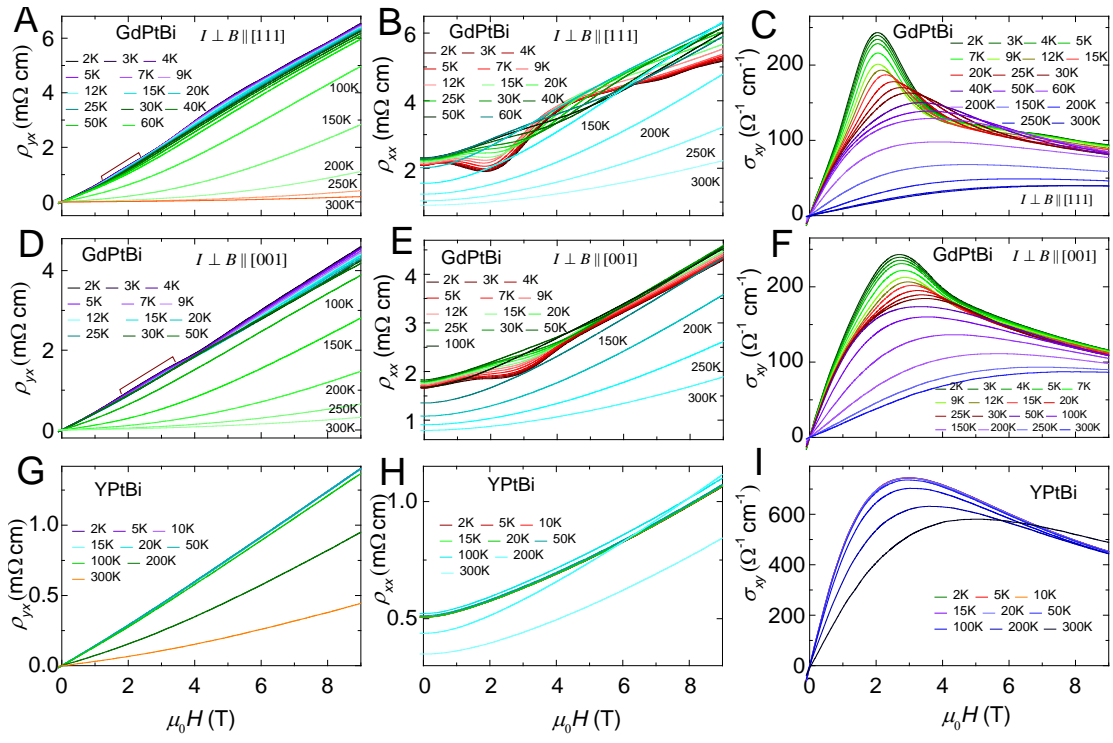


Fig. 2

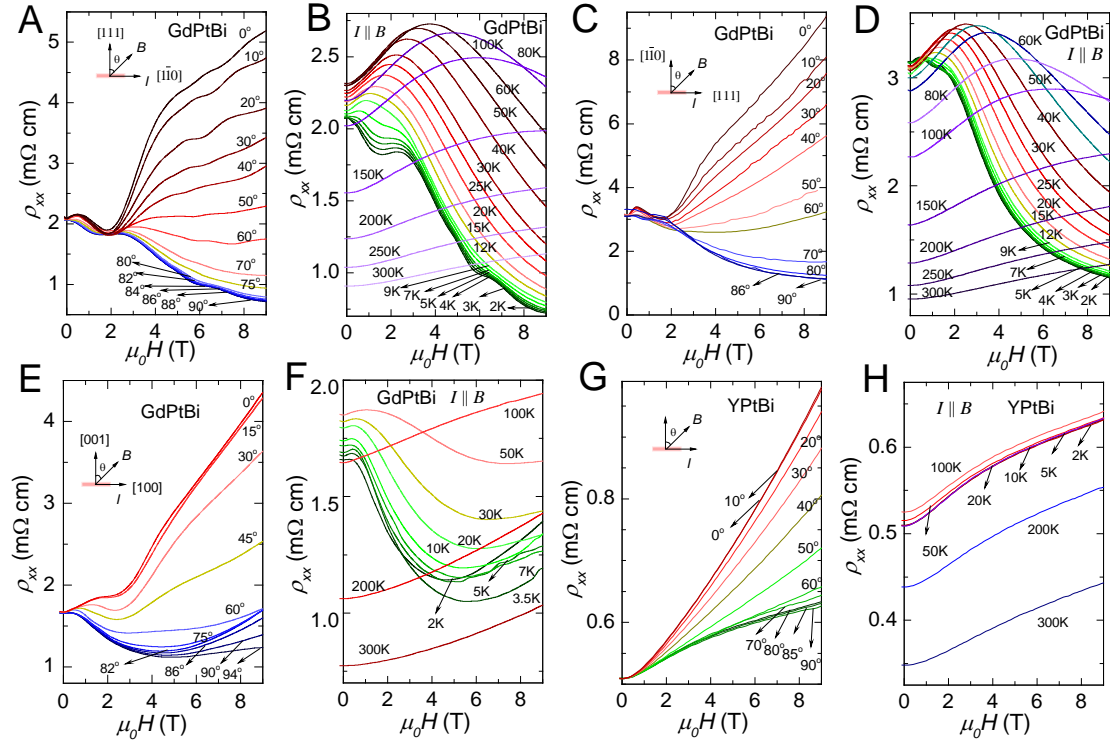


Fig. 3

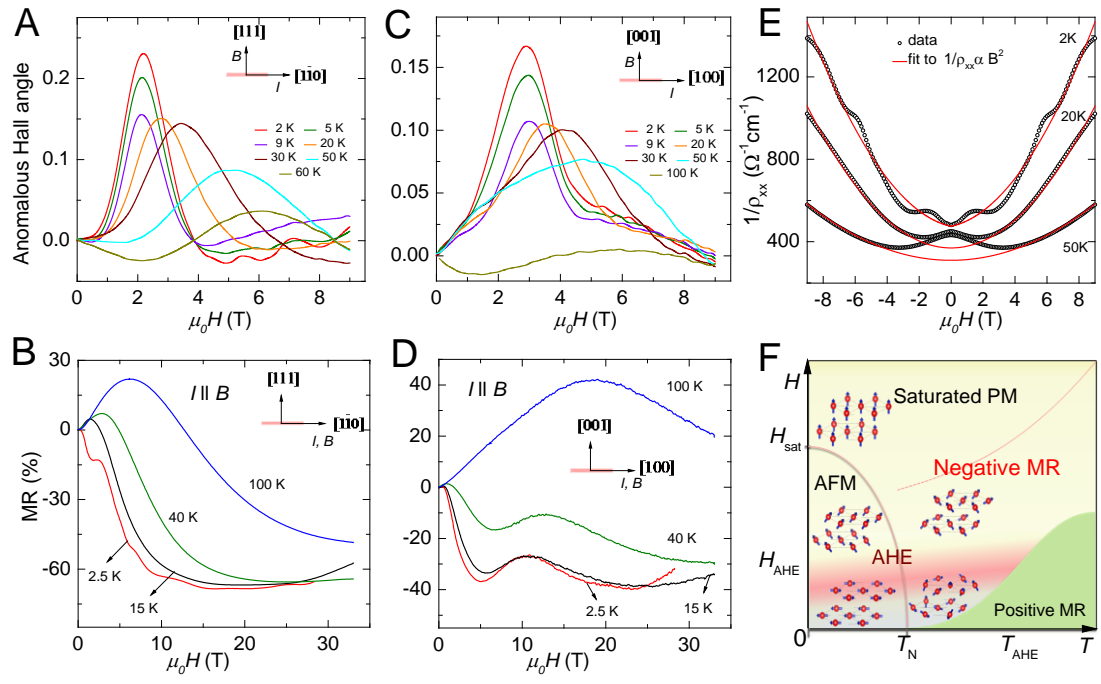


Fig. 4

References

1. X.-L. Qi, S.-C. Zhang, Topological insulators and superconductors. *Rev. Mod. Phys.* **83**, 1057 (2011).
2. M. Z. Hasan, C. L. Kane, *Colloquium: Topological insulators*. *Rev. Mod. Phys.* **82**, 3045 (2010).
3. H. Weng, C. Fang, Z. Fang, B. A. Bernevig, X. Dai, Weyl Semimetal Phase in Noncentrosymmetric Transition-Metal Monophosphides. *Phys. Rev. X* **5**, 011029 (2015).
4. X. Wan, A. M. Turner, A. Vishwanath, S. Y. Savrasov, Topological semimetal and Fermi-arc surface states in the electronic structure of pyrochlore iridates. *Phys. Rev. B* **83**, 205101 (2011).
5. S.-M. Huang *et al.*, A Weyl Fermion semimetal with surface Fermi arcs in the transition metal monpnictide TaAs class. *Nat. Commun.* **6**, (2015).
6. C.-L. Zhang *et al.*, Signatures of the Adler-Bell-Jackiw chiral anomaly in a Weyl fermion semimetal. *Nat. Commun.* **7**, (2016).
7. C. Shekhar *et al.*, Extremely large magnetoresistance and ultrahigh mobility in the topological Weyl semimetal candidate NbP. *Nat. Phys.* **11**, 645 (2015).
8. Z. Wang *et al.*, Dirac semimetal and topological phase transitions in $A_3\text{Bi}$ ($A=\text{Na, K, Rb}$). *Phys. Rev. B* **85**, 195320 (2012).
9. Z. K. Liu *et al.*, Discovery of a Three-Dimensional Topological Dirac Semimetal, Na_3Bi . *Science* **343**, 864 (2014).
10. S. Chadov *et al.*, Tunable multifunctional topological insulators in ternary Heusler compounds. *Nat. Mater.* **9**, 541 (2010).
11. H. Lin *et al.*, Half-Heusler ternary compounds as new multifunctional experimental platforms for topological quantum phenomena. *Nat. Mater.* **9**, 546 (2010).
12. D. Xiao *et al.*, Half-Heusler Compounds as a New Class of Three-Dimensional Topological Insulators. *Phys. Rev. Lett.* **105**, 096404 (2010).
13. Z. Liu *et al.*, Observation of Unusual Topological Surface States in Half-Heusler Compounds LnPtBi ($\text{Ln}=\text{Lu, Y}$). *arXiv:1602.05633*, (2016).
14. M. Hirschberger *et al.*, The chiral anomaly and thermopower of Weyl fermions in the half-Heusler GdPtBi . *arXiv:1602.07219*, (2016).
15. C.-Z. Chang *et al.*, Experimental Observation of the Quantum Anomalous Hall Effect in a Magnetic Topological Insulator. *Science* **340**, 167 (2013).
16. V. Mourik *et al.*, Signatures of Majorana Fermions in Hybrid Superconductor-Semiconductor Nanowire Devices. *Science* **336**, 1003 (2012).

17. A. K. Nayak *et al.*, Design of compensated ferrimagnetic Heusler alloys for giant tunable exchange bias. *Nat. Mater.* **14**, 679 (2015).
18. M. Jourdan *et al.*, Direct observation of half-metallicity in the Heusler compound Co_2MnSi . *Nat. Commun.* **5**, (2014).
19. O. Meshcheriakova *et al.*, Large Noncollinearity and Spin Reorientation in the Mn_2RhSn Heusler Magnet. *Phys. Rev. Lett.* **113**, 087203 (2014).
20. Y. Nakajima *et al.*, Topological RPdBi half-Heusler semimetals: A new family of noncentrosymmetric magnetic superconductors. *Sci. Adv.* **1**, (2015).
21. S. Nakatsuji, N. Kiyohara, T. Higo, Large anomalous Hall effect in a non-collinear antiferromagnet at room temperature. *Nature* **527**, 212 (2015).
22. A. K. Nayak *et al.*, Non-vanishing Berry curvature driven large anomalous Hall effect in non-collinear antiferromagnet Mn_3Ge . *arXiv:1511.03128*, (2015).
23. Z. K. Liu *et al.*, Evolution of the Fermi surface of Weyl semimetals in the transition metal pnictide family. *Nat. Mater.* **15**, 27 (2016).
24. S.-Y. Xu *et al.*, Discovery of a Weyl fermion state with Fermi arcs in niobium arsenide. *Nat. Phys.* **11**, 748 (2015).
25. H. Inoue *et al.*, Quasiparticle interference of the Fermi arcs and surface-bulk connectivity of a Weyl semimetal. *Science* **351**, 1184 (2016).
26. F. Arnold *et al.*, Negative magnetoresistance without well-defined chirality in the Weyl semimetal TaP. *arXiv:1506.06577*, (2015).
27. A. A. Burkov, Anomalous Hall Effect in Weyl Metals. *Phys. Rev. Lett.* **113**, 187202 (2014).
28. A. Kreyssig *et al.*, Magnetic order in GdBiPt studied by x-ray resonant magnetic scattering. *Phys. Rev. B* **84**, 220408 (2011).
29. R. A. Müller *et al.*, Magnetic structure of GdBiPt: A candidate antiferromagnetic topological insulator. *Phys. Rev. B* **90**, 041109 (2014).
30. R. A. Müller *et al.*, Magnetic structure of the antiferromagnetic half-Heusler compound NdBiPt. *Phys. Rev. B* **92**, 184432 (2015).
31. N. Nagaosa, J. Sinova, S. Onoda, A. H. MacDonald, N. P. Ong, Anomalous Hall effect. *Rev. Mod. Phys.* **82**, 1539 (2010).
32. H. Chen, Q. Niu, A. H. MacDonald, Anomalous Hall Effect Arising from Noncollinear Antiferromagnetism. *Phys. Rev. Lett.* **112**, 017205 (2014).
33. P. C. Canfield *et al.*, Magnetism and heavy fermion-like behavior in the RBiPt series. *J. Appl. Phys.* **70**, 5800 (1991).
34. N. P. Butch, P. Syers, K. Kirshenbaum, A. P. Hope, J. Paglione, Superconductivity in the topological semimetal YPtBi. *Phys. Rev. B* **84**, 220504 (2011).

- 35. D. T. Morelli, P. C. Canfield, P. Drymiotis, Low-temperature transport properties of NdBiPt. *Phys. Rev. B* **53**, 12896 (1996).
- 36. G. Kresse, J. Furthmüller, Efficient iterative schemes for *ab-initio* total-energy calculations using a plane-wave basis set. *Phys. Rev. B* **54**, 11169 (1996).
- 37. J. P. Perdew, K. Burke, M. Ernzerhof, Generalized Gradient Approximation Made Simple. *Phys. Rev. Lett.* **77**, 3865 (1996).
- 38. A. A. Mostofi *et al.*, wannier90: A tool for obtaining maximally-localised Wannier functions. *Comput. Phys. Commun.* **178**, 685 (2008).